crystals

MDPI

Article

The Electrochemical Reduction Mechanism of $ZnFe_2O_4$ in NaCl-$CaCl_2$ Melts

Chang Liu, Jinglong Liang, Hui Li *, Hongyan Yan, Sijia Zheng, Weigang Cao and Le Wang

College of Metallurgy and Energy, North China University of Science and Technology, Tangshan 063210, China; lc15373501009@126.com (C.L.); ljl@ncst.edu.cn (J.L.); yanhy@ncst.edu.cn (H.Y.); zhengsijia@ncst.edu.cn (S.Z.); caoweigang@ncst.edu.cn (W.C.); wangl@ncst.edu.cn (L.W.)
* Correspondence: lh@ncst.edu.cn

Abstract: The electrochemical reduction process of $ZnFe_2O_4$ in NaCl-$CaCl_2$ melts was studied. Thermodynamic analysis shows that the reduction process of $ZnFe_2O_4$ is carried out in multiple steps, and it is difficult to reduce Fe^{3+} to Fe in one step. Electrochemical tests revealed that the reduction process of $ZnFe_2O_4$ includes three steps: First, Fe^{3+} is reduced to Fe in two steps, then Zn^{2+} is reduced to Zn in one step. The reduction of Fe^{3+} on the Mo electrode is a reversible process controlled by diffusion, while the reduction of Zn^{2+} is an irreversible process controlled by diffusion. The influence of electrolysis voltage and temperature on the process of electric deoxidation has also been studied. It is indicated that properly increasing the temperature is conducive to the diffusion of oxygen ions, thereby increasing the deoxidation rate. With the gradual increase of voltage, the reduction process of $ZnFe_2O_4$ is $ZnFe_2O_4 \rightarrow FeO + ZnO \rightarrow Fe + ZnO \rightarrow Fe + Zn$.

Keywords: zinc ferrite; thermodynamics research; melts electrochemistry; electro-deoxidation

Citation: Liu, C.; Liang, J.; Li, H.; Yan, H.; Zheng, S.; Cao, W.; Wang, L. The Electrochemical Reduction Mechanism of $ZnFe_2O_4$ in NaCl-$CaCl_2$ Melts. *Crystals* **2021**, *11*, 925. https://doi.org/10.3390/cryst11080925

Academic Editor: Dmitry Medvedev

Received: 20 July 2021
Accepted: 5 August 2021
Published: 9 August 2021

1. Introduction

Lots of solid slag containing $ZnFe_2O_4$ are inevitably produced in the process of zinc metallurgy [1,2]. $ZnFe_2O_4$ can cause a low zinc leaching rate in zinc hydrometallurgy. The massive accumulation of these solid residues also causes serious waste of resources and pollution to the air and soil [3]. Therefore, $ZnFe_2O_4$ in the waste can not only be reused as a resource, but is significant for environmental protection.

In order to obtain zinc and iron, $ZnFe_2O_4$ is subjected to zinc-iron separation by electro-deoxidation in melts [4,5]. This process can realize the reduction and extraction of two metals from the waste residue. Moreover, when preparing target products with high cost, high melting point, and difficult to shape, this process can effectively reduce the difficulty of preparation. Because of the electrolysis process carried out in the solid oxide, even if the melting point of the two metals in the product is quite different, the desired alloy can still be prepared [6]. In addition, the operation method is convenient and the equipment is easy, the production time is short, and the equipment is reduced. At present, the process can prepare a lot of products in the laboratory stage, but more research is needed to produce them on a large scale. Thermodynamic analysis and electrochemical testing methods are applied to explore the electrochemical mechanism of zinc and iron separation in melts. The reduction process of melts electrolysis $ZnFe_2O_4$ is studied.

2. Experimental

This experiment used NaCl-$CaCl_2$ melts, the reason is the theoretical decomposition voltage of this system is relatively high, the theoretical decomposition voltage of NaCl is −3.24 V, and the $CaCl_2$ is −3.29 V. The system has good conductivity, which is conducive to the progress of electrolytic deoxidation. The eutectic temperature is approximately 500 °C and below the experimental temperature [7].

2.1. Experimental Materials

The NaCl, $CaCl_2$ and $ZnFe_2O_4$ are analytically pure. The ratio of NaCl and $CaCl_2$ was 1:1. The reagents were dried at 200 °C for 8 h using DZF-6050 electric vacuum drying oven and cooled down to room temperature.

2.2. Experimental Method

2.2.1. Electrochemical Experiment

The CHI660E electrochemical workstation was used for experimental testing, and the reduction mechanism of $ZnFe_2O_4$ was analyzed by cyclic voltammetry (CV), square wave voltammetry (SWV), and open circuit potential (OCPT). The experiment used a three-electrode system, the working electrode was Mo wire (Φ0.5 mm) which was coated by $ZnFe_2O_4$ powder 3 g of $ZnFe_2O_4$ powders are added to 5 mL of alcohol to make a suspension, then immerse the Mo wire in the suspension for 15 min; A Ag/Ag^+ reference electrode was prepared by filling an aluminum silicate tube (Φ5 mm) with a molar ratio of NaCl: $CaCl_2$: AgCl = 46: 50: 4 and silver wire (Φ0.5 mm, 99.99%); High-purity graphite flakes with good conductivity (99.99%, 80 mm × 20 mm × 5 mm) was polished with sandpaper, cleaned and dried with alcohol, a nickel wire is used to connect the graphite and flakes with Φ5 mm stainless steel rod as anode. Three-electrode system diagram is shown in Figure 1. All experiments were carried out under high purity argon (>99.999%).

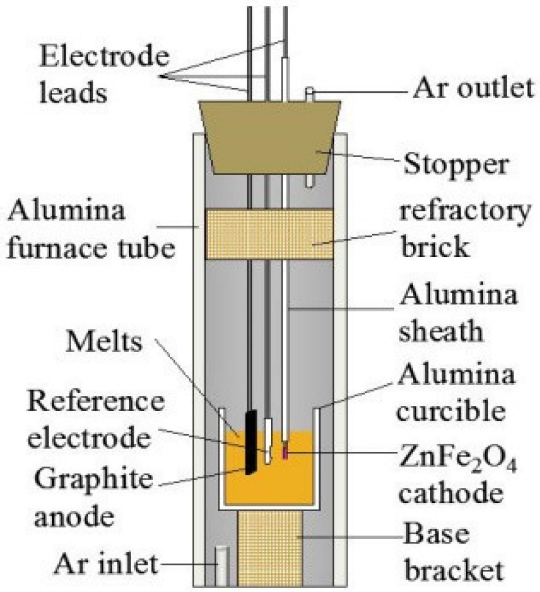

Figure 1. Three-electrode system diagram.

The electrolyte was composed of $CaCl_2$ and NaCl. According to n ($CaCl_2$): n (NaCl) = 1:1 prepare 200 g. It was well mixed into the corundum crucible [8–10] and put the crucible into the tubular resistance heating furnace. Raised the temperature to 800 °C at 8 °C·min^{-1}, keep constant temperature for 1 h. Heating process under the protection of high-purity argon gas (>99.99%). The three electrodes are put into NaCl-$CaCl_2$ melts (the cathode is immersed in the melts depth of 2 mm, the anode is immersed in the meltsdepth of 20 mm), the electrochemical reduction behavior of $ZnFe_2O_4$ on the Mo working electrode is measured, and the reversibility of the reduction process and the number of transferred electrons are measured analyze.

2.2.2. $ZnFe_2O_4$ Electrolysis Experiment

The electrolysis experiment is used a two-electrode system, and the GWINSTEK PSM-3004 DC power supply is used to carry out the constant cell pressure electrolysis experiment. The cathode was prepared by grinding $ZnFe_2O_4$ powder and pressed it

under a pressure of 200 MPa to form a $ZnFe_2O_4$ cylindrical sheet with diameter of 15 mm, thickness of 3 mm and weight of 1.2 g, which was placed in a tubular resistance furnace and sintered at 800 °C for 5 h to obtain sufficient mechanical strength. After cooling, it was wrapped with stainless steel mesh and connected with an iron rod to form a wire collector. The preparation of graphite anode is the same as the electrochemical test experiment.

The sample was slowly cooled with argon gas to 25 °C after the end of electrolysis, and the electrolysis product was ultrasonically washed in a beaker containing alcohol for 30 min. Characterization of the sample was analyzed by X-ray diffraction spectroscopy (XRD, X-ray 6000 with Cu Kα1 radiation λ = 1.5405 Å), scanning electron microscopy (SEM, JEM-2800F) and energy dispersive spectroscopy (EDX, EDAX Genesis 7000).

The schematic diagram of the electrode and the electrolysis device are shown in Figure 2.

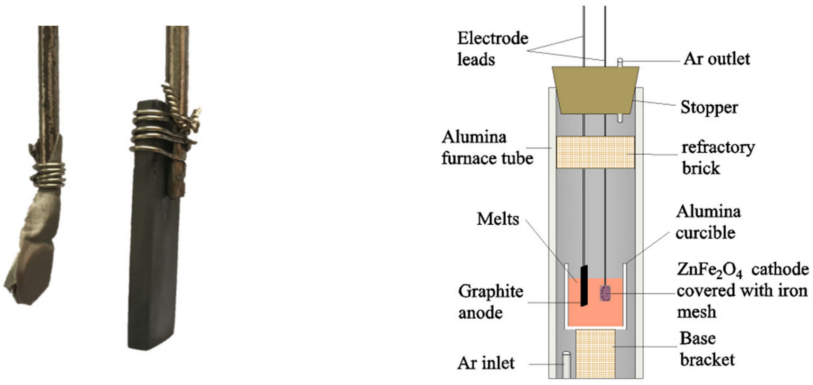

Figure 2. Physical picture of electrode and schematic diagram of electrolysis device.

3. Results and Discussion

3.1. The Calculation of Decomposition Voltage and Oxygen Partial Pressure of $ZnFe_2O_4$

The theoretical decomposition voltage E^{Θ} of $ZnFe_2O_4$ was calculated by Formula (1) [11].

$$\Delta G^{\Theta} = -nFE^{\Theta} \quad (1)$$

where ΔG^{Θ} (kJ·mol^{-1}) is the standard Gibbs free energy; n is the number of exchanged electrons; F (96485C·mol^{-1}) is the Faraday's constant.

LgP_{O_2} was calculated by Formula (2) to analyze the difficulty of $ZnFe_2O_4$ reduction in stages.

$$\Delta G^{\Theta} = -2.303RT\lg P_{O_2} \quad (2)$$

where ΔG^{Θ} (kJ·mol^{-1}) is the standard Gibbs free energy; R (8.314 J·mol^{-1}·K^{-1}) is the molar gas constant; T (K) is the temperature; $\lg P_{O_2}$ is the oxygen partial pressure.

The more positive the theoretical reduction voltage of the metal, the easier it will be reduced. It can be seen from Figure 3a that the first reaction is $2ZnFe_2O_4 = 4FeO + 2ZnO + O_2$ (g), the reduction products are mainly FeO and ZnO. Then, $2FeO = 2Fe + O_2$ (g) and $2ZnO = 2Zn + O_2$ (g) are occurred successively. Therefore, the reduction process of Fe in $ZnFe_2O_4$ is carried out in steps.

Figure 3b shows that the reaction $ZnFe_2O_4 = 2Fe + ZnO + 1.5O_2$ (g) has the lowest oxygen partial pressure, compared with stepwise reduction to Fe from $ZnFe_2O_4$, the conditions of one-step are more complicated. Therefore, under a certain oxygen partial pressure, $ZnFe_2O_4$ should first be reduced to FeO, then the reaction of FeO to Fe and ZnO to Zn are carried out successively.

The reduction process of $ZnFe_2O_4$ is carried out by multiple steps, which provides the basis for the following electrochemical test analysis and electro-deoxidation experiment.

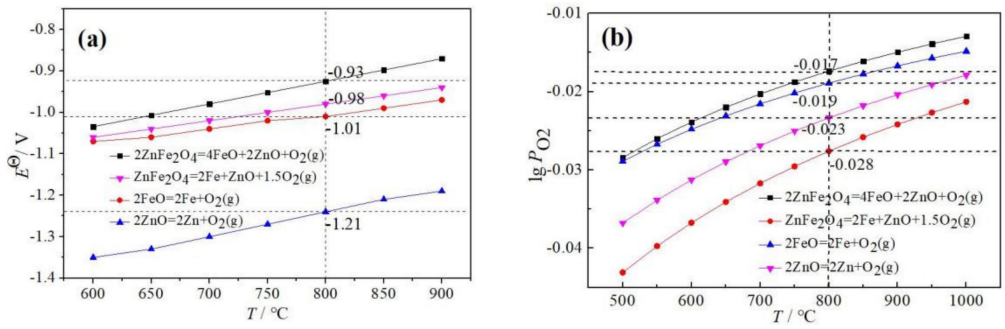

Figure 3. (**a**) The relationship between the theoretical decomposition voltage and temperature of $ZnFe_2O_4$, (**b**) the relationship between the oxygen partial pressure and temperature of $ZnFe_2O_4$.

3.2. Electrochemical Analysis of $ZnFe_2O_4$ in Melts

3.2.1. Cyclic Voltammetry

The reduction mechanism of $ZnFe_2O_4$ in NaCl-$CaCl_2$ melts was studied by CV, which was shown in Figure 4. Figure 4a is comparison chart of CV without and with $ZnFe_2O_4$, scan rate was 0.3 V·s^{-1}. The peak D and peak D shown by the dotted line were the oxidation and reduction processes of Na, and the peak E was the oxidation of chlorine inos [12].

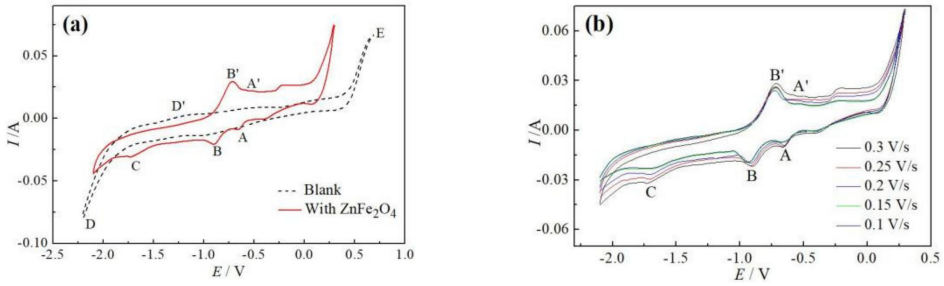

Figure 4. CV curves on Mo electrode at 800 °C (**a**) a scan rate of 0.3 V·s^{-1} and (**b**) with different scanning rates (0.1 V·s^{-1}~0.3 V·s^{-1}).

In the electric potential range between −2.1 V and 0.3 V, Mo electrode coated with $ZnFe_2O_4$ powder, CV curves at different scan rates were shown in Figure 4b. Peak A (−0.7 V), Peak B (−0.9 V) and Peak C (−1.7 V) represent the three reduction processes, the oxidation peak A′ and peak B′ corresponding to the reduction peak A and peak B. The E_{pc} of peak A and peak B did not shift significantly with the increase of scanning speed, while the E_{pc} of peak C shifted. Therefore, it could be seen that peak A and peak B were reversible reaction processes [13,14], and peak C was an irreversible reaction process [15,16]. The relationship between $i_{pc} \sim v^{1/2}$ was calculated by the data of peak A, peak B and peak C as shown in Figure 5. The linear relationship between i_{pc} and $v^{1/2}$ indicated that the electrochemical reactions of peak A, peak B, and peak C were all diffusion-controlled reactions [12,17,18].

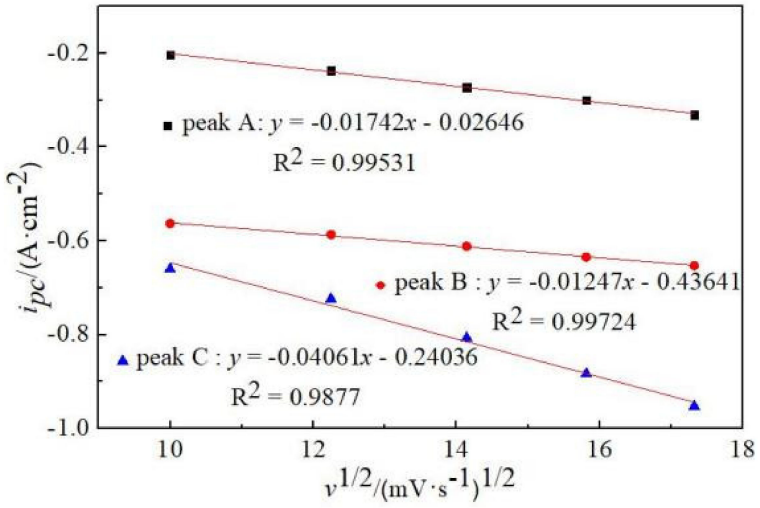

Figure 5. $ZnFe_2O_4$ coated Mo electrode i_{pc} and $v^{1/2}$ relationship curve.

The number of exchanged electrons in the reduction reaction of peak A and peak B can be calculated by Formula (3) [13,14].

$$E_{pc} - E_{pc/2} = -0.77(RT/nF) \quad (3)$$

where E_{pc} (V) is the cathodic peak potential; $E_{pc/2}$ (V) is the half-peak potential; n is the number of exchanged electrons; F(96485C·mol^{-1}) is the Faraday's constant; R(8.314 J·mol^{-1}·K^{-1}) is the molar gas constant; T(1073 K) is the temperature.

The average value of $E_{pc} - E_{pc/2}$ under different scanning speeds of peak A was −0.05538 V, the n value was 1.28 (≈1) for peak A. The average value of $E_{pc} - E_{pc/2}$ under different scanning speeds of peak B was −0.04 V, the n value was 1.78 (≈2) for peak B. Therefore, peak C was the reduction of Zn, $ZnFe_2O_4$ undergoes three-step reduction on the Mo electrode.

3.2.2. Square Wave Voltammetry and Open Circuit Potential

SWV and OCPT were used to study the electrochemical reduction behavior of $ZnFe_2O_4$ deoxidation on the Mo electrode in NaCl-$CaCl_2$ melts, the experimental data is shown in Figure 6.

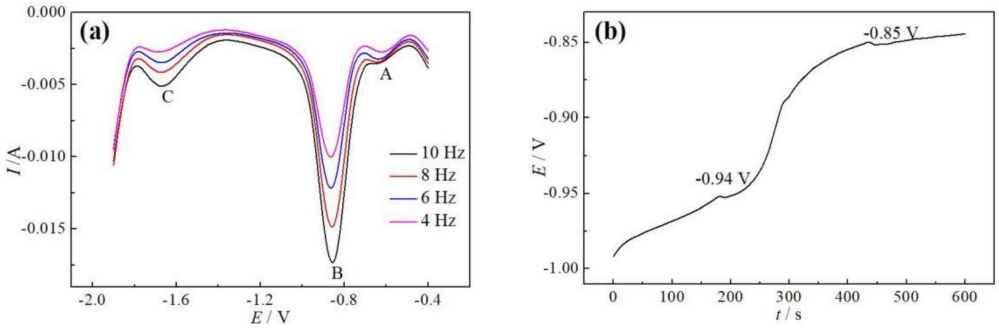

Figure 6. (**a**) SWV curves and (**b**) OCPT curve on Mo electrode (f: 4~10 Hz, T = 800 °C).

Three obvious reduction peak A (−0.62 V), peak B (−0.86 V) and peak C (−1.67 V) appeared on the curves in Figure 6a. Combining with CV, the peak A and peak B correspond to the two-step reduction reaction of Fe^{3+} on the Mo electrode, peak C was a one-step reduction of Zn^{2+}. The stepwise reduction behavior of Fe^{3+} was studied by OCPT measurements, as shown in Figure 6b. An obvious platform appeared at −0.85 V, which

was corresponding to the reaction of $Fe^{3+} \rightarrow Fe^{2+}$. Another platform appeared near −0.94 V, which was the reaction of $Fe^{2+} \rightarrow Fe$.

For the reversible reaction of diffusion control, the relationship between i_{pc} and $f^{1/2}$ can be calculated using Formula (4).

$$i_{pc} = -031\pi^{-1/2}R^{-1}T^{-1}AC_0D^{1/2}n^2F^2\Delta Ef^{1/2} \quad (4)$$

where i_{pc}(A) is the cathodic peak current; A(cm^2) is the area of electrode; C_0($mol \cdot cm^{-3}$) is the molar concentration of electroactive species; D($cm^3 \cdot s^{-1}$) is the diffusion coefficient of electroactive species; ΔE(V) is the potential amplitude; $f^{1/2}$ is the square root of the formula.

Theoretically, the linear relationship between i_{pc} and $f^{1/2}$ should pass through the origin [19–21]. However, some studies had found that the straight line fitted by the experimental data points will be shifted. There are two main reasons [22,23]. On the one hand, the electrode reaction will be accompanied by some other reaction processes. When fitting the experimental data points to a straight line, it will result in a small positive intercept. It cannot be denied that the process is affected by diffusion control due to the presence of a positive intercept. On the other hand, there is a certain experimental error. In order to reduce the error, the origin and experimental data points were put together to fit a straight line. Some researchers had also adopted this method [24–26].

It could be seen from Figure 7, the E_{pc} of peak A and peak B did not shift significantly, which further indicates that peak A and peak B were reversible reactions.

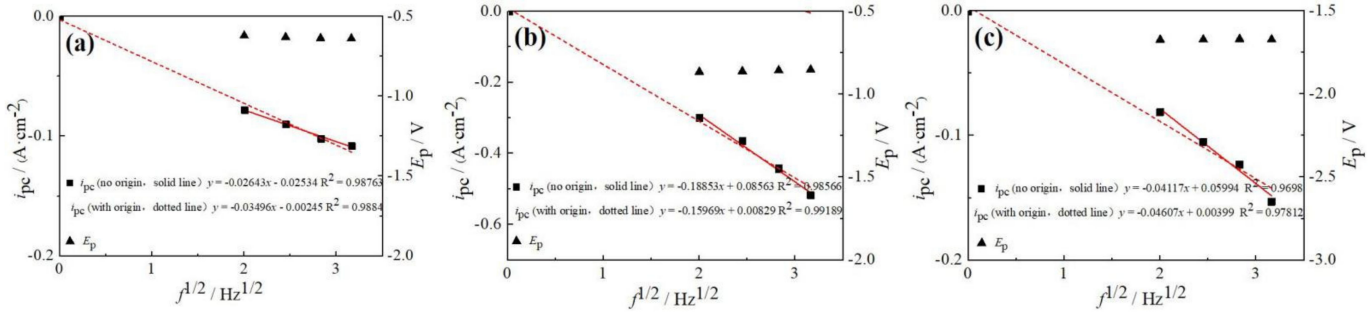

Figure 7. Correlation between peak current (i_{pc}), peak potential (E_{pc}) and square root of formula ($f^{1/2}$) of (**a**) peak A, (**b**) peak B and (**c**) peak C.

Because of other reaction processes and experimental errors, the experimental data of peak current density (including and excluding the origin) were fitted in this study [24], as shown in Figure 7. The ratio of the diffusion coefficients can be obtained from the slope of the linear fit. D_1/D_2 of peak A = 0.5715, D_1/D_2 of peak B = 1.393, D_1/D_2 of peak C = 0.8368. There was a little difference between the values of D_1 & D_2 which was in the same magnitude. Therefore, the number of exchanged electrons of $ZnFe_2O_4$ can be calculated according to the Formula (5) [27].

$$W_{1/2} = 3.52RT/nF \quad (5)$$

where $W_{1/2}$(V) is the half-peak width.

The n value was 1.41 (≈1) for peak A, 2.04(≈2) for peak B, and 1.55 (≈2) for peak C. The calculation result was the same as the CV. Therefore, the step-reduction process of $ZnFe_2O_4$ is $ZnFe_2O_4 \rightarrow FeO + ZnO \rightarrow Fe + ZnO \rightarrow Fe + Zn$.

3.3. The Electrolysis of $ZnFe_2O_4$ in Melts

3.3.1. Product Analysis under Different Electrolytic Voltages

According to the above electrochemical tests, the reduction process of Fe^{3+} in $ZnFe_2O_4$ was a two-step reduction, and the reduction process of Zn^{2+} was a one-step reduction. The

melts temperature was 800 °C and different electrolysis voltages (0.6 V, 0.8 V, 1.0 V, 1.2 V, 1.6 V, 1.8 V) were used.

It can be seen from Figure 8 that in the voltage range of 0.6 V~1 V, the main products were FeO and ZnO, which corresponds to the first reduction reaction of $ZnFe_2O_4$. The crystal structure of ZnO had changed at 1 V, the structure of cubic sphalerite (a = 0.428 nm) gradually changed to hexagonal red zincite (a = 0.325 nm, b = 0.521 nm) [28].

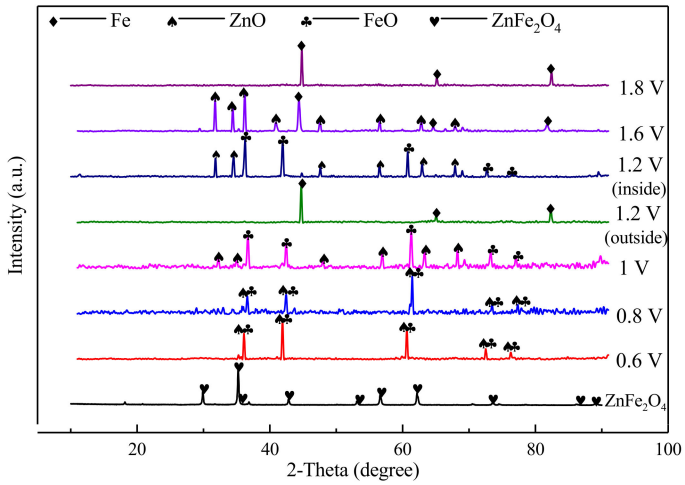

Figure 8. XRD of products at different electrolysis voltages (E = 0.6 V~1.8 V, T = 800 °C, t = 8 h).

According to XRD at 1.2 V, the main substance of metal shell was iron, the internal components were mainly FeO and ZnO, as shown in Figure 9a. Therefore, when the electrolysis voltage was 1.2 V, the reduction reactions of $ZnFe_2O_4$ from outside to inside were $ZnFe_2O_4 \rightarrow FeO \rightarrow Fe$. The product was a dense dark brown hard solid at 1.6 V, as shown in Figure 9b. It can be observed that there was a little black irregular solid embedded in the metal shell inside the product, the product obtained by the 1.6 V was mainly Fe and ZnO. In the voltage range of 1.2 V~1.6 V, the same reaction occurs at different electrolytic voltages, but the morphology of the products differs greatly. Electrolysis first occurs on the surface of massive $ZnFe_2O_4$, forming a three-phase interface of melts, stainless steel mesh and $ZnFe_2O_4$. While the reaction proceeds, the three-phase interface expands from the surface to the inside, and oxygen ions were precipitated, forming a new three-phase interface of melts, metal and solid oxygen-containing compound [29–31].

(**a**) (**b**)

Figure 9. Physical of products at (**a**) 1.2 V and (**b**) 1.6 V (T = 800 °C, t = 8 h).

Figure 8 shows that the main product at 1.8 V was Fe. It indicated that the reduction reaction were $ZnFe_2O_4 \rightarrow FeO \rightarrow Fe$ and $ZnO \rightarrow Zn$. Figure 10 shows the SEM and EDS images of the cathode product at 1.8 V. It can be seen that the particle size of the product was uniform. Fe atoms formed by the reduction of Fe^{3+} aggregate to form crystal nuclei with crystal structure, the crystal particles continue to grow with the reduction process to form metallic Fe with a certain particle size, and the Fe grains form a loose and porous structure during the growth process. According to EDS analysis, the atomic percentages of

Fe and Zn were 95.19% and 0.86% respectively, the atomic percentage of O was 3.95%. It indicated that a good deoxidation effect can be achieved at 1.8 V after 8 h of electrolysis. The driving force of electrical deoxidation increases with increasing voltage [32], and the reduction of Fe^{3+} and Zn^{2+} is easier.

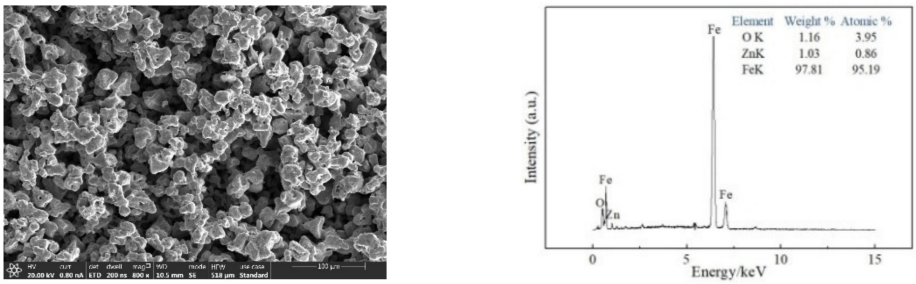

(**a**) (**b**)

Figure 10. (**a**) SEM and (**b**) EDS diagrams of products at 1.8 V electrolysis voltage (T = 800 °C, t = 8 h).

3.3.2. Zinc Behavior during the Electrolysis of $ZnFe_2O_4$

There was no Zn detected in the product at 1.8 V, because the experimental temperature (800 °C) was closed to the boiling temperature of Zn (907 °C), and Zn has a significant vapor pressure at a temperature below the boiling point [33]. If zinc was reduced, a small part of the Zn had sunk to the bottom of the melts. A greater part of it would become zinc vapor volatilization, so the content of zinc in the product was less.

In order to study the behavior of Zn during electrolysis, a method will be adopted [34]. The $ZnFe_2O_4$ powder was placed in a small graphite crucible and electrically deoxidized for collecting the Zn, as shown in Figure 11a. After the electrical deoxidation was over, the product was taken out and cleaned, and the bottom of the product was detected by XRD. Figure 11b is the XRD analysis results, in addition to Zn, the presence of ZnO was also detected.

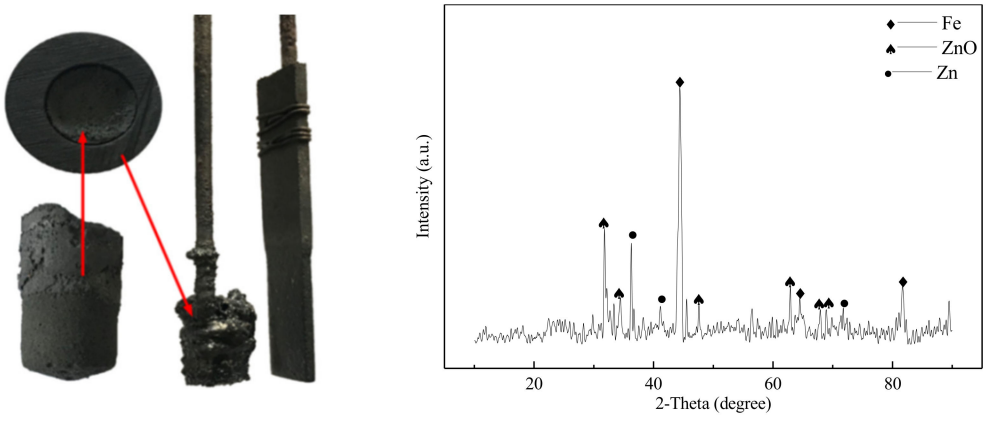

(**a**) (**b**)

Figure 11. (**a**) Experimental physical diagram and (**b**) XRD analysis diagram (E = 1.8 V, T = 800 °C, t = 8 h).

3.3.3. Product Analysis at Different Electrolytic Temperatures

When the temperature is the only variable, the diffusion rate of oxygen ions is mainly affected by the temperature, and the changed temperature would also affect the viscosity and conductivity of the melts. Therefore, the temperature of the melts in the electrolysis process is an important parameter [35], which would affect the deoxidation rate and deoxidation effect.

Figures 12 and 13 are the XRD & SEM of the electrolytic products, which show that the main products were Fe and ZnO at 700 °C, the ZnO and Fe particles were bound to each other to form a relatively dense structure, indicating that the deoxidation of $ZnFe_2O_4$ was not complete. At 750 °C and 800 °C, the products were Fe. At 800 °C, the diffraction peak of XRD was sharper, indicating that the crystalline state of iron was better and Fe particle size increases. Figure 13 shows that the product had a larger particle size and pore spacing at 800 °C, which is more conducive to deoxidation. According to EDS spectrum analysis, the change of each element content with increasing temperature was shown in Figure 14, the atomic percentage of Fe was 95.19% at 800 °C, which had a lower oxygen content and zinc content than 86.55% at 750 °C. Therefore, the deoxidation effect is better at 800 °C. Within a suitable temperature range, as the temperature increases, the activation energy and diffusion coefficient are greater, and the viscosity of melts can be reduced, thereby increasing the reaction rate [36].

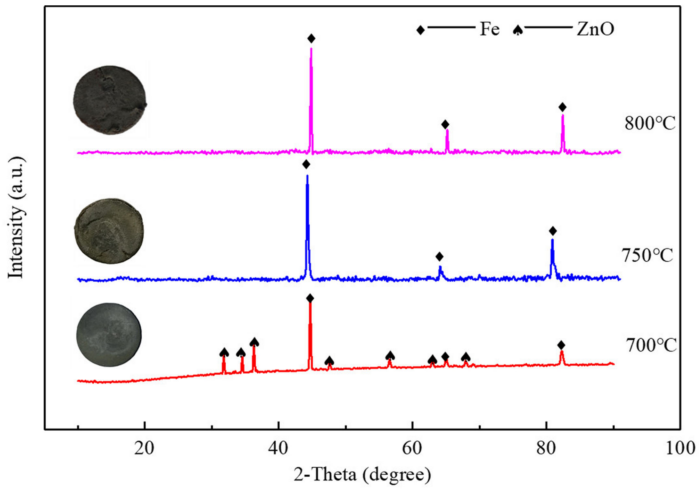

Figure 12. XRD patterns of cathode products at different electrolysis temperatures (E = 1.8 V, t = 8 h).

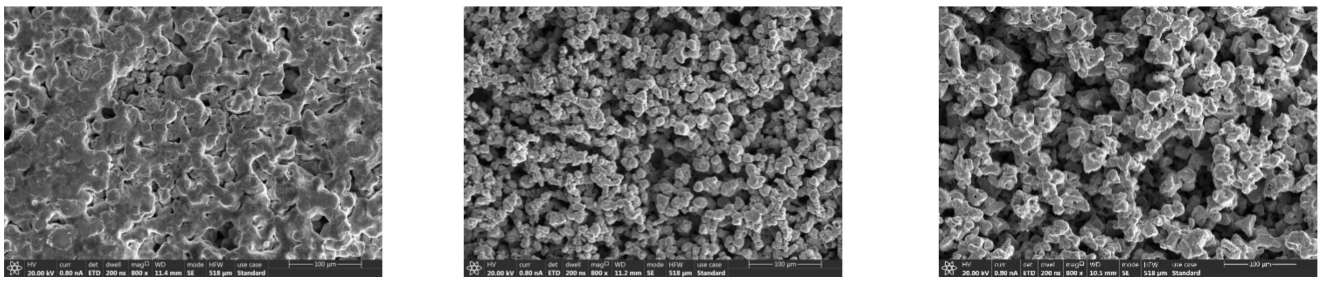

(**a**) (**b**) (**c**)

Figure 13. SEM of cathode products at (**a**) 700 °C, (**b**) 750 °C and (**c**) 800 °C (E = 1.8 V, t = 8 h).

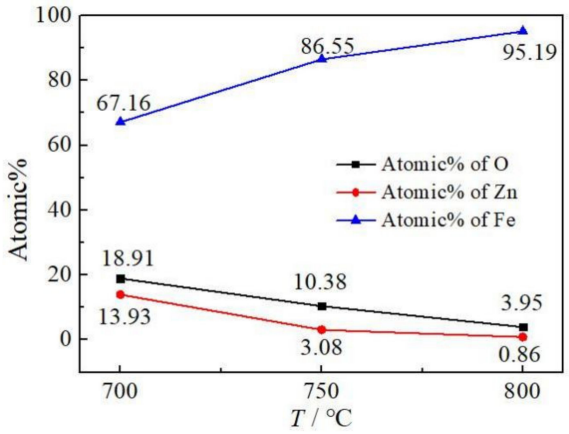

Figure 14. The relationship between the content of each element as the temperature increases (E = 1.8 V, t = 8 h).

4. Conclusions

(1) The electrochemical reduction process of $ZnFe_2O_4$ on the Mo electrode is a three-step reduction: $ZnFe_2O_4 \rightarrow FeO + ZnO \rightarrow Fe + ZnO \rightarrow Fe + Zn$. $Fe^{3+} \rightarrow Fe^{2+} \rightarrow Fe$ are reversible reduction processes controlled by diffusion, and $Zn^{2+} \rightarrow Zn$ is an irreversible reduction process controlled by diffusion.

(2) The surface of the deoxidized product has high crystallinity at 1.8 V electrolysis for 8 h. The lower content of Zn and O indicates that the deoxidation effect is better.

(3) Electrolysis voltage is the driving force for electro-deoxidation, $ZnFe_2O_4$ is reduced to FeO and ZnO during the voltage of 0.6 V~1 V, then FeO is reduced to Fe at 1.2 V~1.6 V, when the electrolysis voltage is 1.8 V, ZnO is also reduced to Zn. The increase of temperature is beneficial to the diffusion of oxygen ions, the deoxidation rate is accelerated and the occurrence of side reactions can be reduced.

(4) Electrolysis experiments also verified the stepwise reduction of $ZnFe_2O_4$. The reduction of $ZnFe_2O_4$ is achieved by electrolysis at 800 °C and 1.8 V for 8 h.

Author Contributions: Conceptualization, C.L. and H.L.; data curation, J.L.; writing—original draft preparation, H.Y. and S.Z.; writing—review and editing, W.C.; visualization, L.W. All authors have read and agreed to the published version of the manuscript.

Funding: This research was funded by the National Natural Science Foundation of China, grant number 51874141.

Conflicts of Interest: The authors declare no conflict of interest.

References

1. Chen, T.T.; Dutrizac, J.E. Mineralogical changes occurring during the fluid-bed roasting of zinc sulfide concentrates. *JOM* **2004**, *56*, 46–54. [CrossRef]
2. Kim, W.; Saito, F. Mechanochemical synthesis of zinc ferrite from zinc oxide and α-Fe_2O_3. *Powder Technol.* **2001**, *114*, 12–16. [CrossRef]
3. Zhang, Y.J.; Li, X.H.; Pan, L.; Wei, Y.S.; Liang, X.Y. Effect of mechanical activation on the kinetics of extracting indium from indium-bearing zinc ferrite. *Hydrometallurgy* **2010**, *102*, 95–100. [CrossRef]
4. Chen, Z.; Fray, D.J.; Farthing, T.W. Direct electrochemical reduction of titanium dioxide to titanium in molten calcium chloride. *Nature* **2000**, *407*, 361–364. [CrossRef] [PubMed]
5. Kartal, L.; Daryal, M.B.; Sireli, G.K.; Timur, S. One-step electrochemical reduction of stibnite concentrate in molten borax. *Int. J. Miner. Metall. Mater.* **2019**, *26*, 1258–1265. [CrossRef]
6. Schwandt, C.; Doughty, G.R.; Fray, D.J. The FFC-Cambridge process for titanium metal winning. *Key Eng. Mater.* **2010**, *436*, 13–25. [CrossRef]
7. Xiong, L.; Hua, Y.X.; Xu, C.Y.; Li, Y.; Zhang, Q.B.; Zhou, Z.; Zhang, Y.D.; Yu, J.J. Effect of CaO addition on preparation of ferrotitanium from ilmenite by electrochemical reduction in $CaCl_2$-NaCl molten salt. *J. Alloy. Compd.* **2016**, *676*, 383–389. [CrossRef]

8. Lzyumskaya, N.; Tahira, A.; Ibupoto, Z.H.; Lewinski, N.; Avrutin, V.; Özgür, Ü.; Topsakal, E.; Willander, M.; Morkoç, H. Review—Electrochemical Biosensors Based on ZnO Nanostructures. *ECS J. Solid State Sci. Technol.* **2017**, *6*, 84–100. [CrossRef]
9. Peng, J.J.; Li, G.M.; Chen, H.L.; Wang, D.H.; Jin, X.B.; Chen, G.Z. Cyclic Voltammetry of ZrO_2 Powder in the Metallic Cavity Electrode in Molten $CaCl_2$. *J. Electrochem. Soc.* **2010**, *157*, F1. [CrossRef]
10. Lebedev, V.A.; Sal'Nikov, V.I.; Tarabaev, M.V.; Sizikov, I.A.; Rymkevich, D.A. Kinetics and mechanism of the processes occurring at graphite anode in a CaO-$CaCl_2$ melt. *Russ. J. Appl. Chem.* **2007**, *80*, 1498–1502. [CrossRef]
11. Weng, W.; Wang, M.Y.; Gong, X.Z.; Wang, D.; Guo, Z.H. Electrochemical reduction behavior of soluble $CaTiO_3$ in Na_3AlF_6-AlF_3 melt for the preparation of metal titanium. *J. Electrochem. Soc.* **2017**, *164*, 551–557. [CrossRef]
12. Xiao, S.J.; Liu, W.; Gao, L. Cathodic process of manganese (II) in NaCl-KCl melt. *Ionics* **2016**, *22*, 2387–2390. [CrossRef]
13. Ghallali, H.E.; Groult, H.; Barhoun, K.; Krulic, D.; Lantelme, F. Lantelme, Electrochemical synthesis of Ni–Sn alloys in molten LiCl–KCl. *Electrochim. Acta* **2009**, *54*, 3152–3160. [CrossRef]
14. Vandarkuzhali, S.; Gogoi, N.; Ghosh, S.; Reddy, B.P.; Nagarajan, K. Electrochemical behaviour of LaCl3 at tungsten and Aluminium cathodes in LiCl–KCl eutectic melt. *Electrochim. Acta* **2012**, *59*, 245–255. [CrossRef]
15. Rezaei, M.; Ghorbani, M.; Dolati, A. Electrochemical investigation of electrodeposited Fe–Pd alloy thin films. *Electrochim. Acta* **2010**, *56*, 483–490. [CrossRef]
16. Kuznetsov, S.A.; Hayashi, H.; Minato, K.; Eacard, M.G. Electrochemical transient techniques for determination of uranium and rare-earth metal separation coefficients in molten salts. *Electrochim. Acta* **2006**, *51*, 2463–2470. [CrossRef]
17. Wei, L.; Sai, J.X.; Zhen, W. Electrochemical Behavior of Cr(II) Ion in NaCl-KCl Melt at W Electrode. *Int. J. Electrochem. Sci.* **2017**, *17*, 119–122.
18. Li, M.; Liu, B.; Ji, N. Electrochemical extracting variable valence ytterbium from LiCl–KCl–$YbCl_3$ melt on Cu electrode. *Electrochim. Acta* **2016**, *193*, 54–62. [CrossRef]
19. Wiedenroth, A. The Fe^{2+}/Fe^{3+}-redox equilibrium in $5Na_2O{\cdot}15CaO{\cdot}xAl_2O_3{\cdot}(80-x)SiO_2$(x = 5 − 25) liquids. *J. Non-Cryst. Solids.* **2001**, *290*, 41–48. [CrossRef]
20. Ruessel, C.; Freude, E. Voltammetric studies in a soda-lime-silica glass melt containing two different polyvalent ions. *Glastech. Ber.* **1990**, *63*, 149–153.
21. Claussen, O.; Ruessel, C. Quantitative in-situ determination of iron in a soda-lime-silica glass melt with the aid of square-wave voltammetry. *Glastech. Ber. Glass Sci. Technol.* **1996**, *69*, 95–100.
22. Lugovskoy, A.; Zinigrad, M.; Aurbach, D.; Unger, Z. Electrodeposition of iron(II) on platinum in chloride melts at 700–750 °C. *Electrochim. Acta* **2009**, *54*, 1904–1908. [CrossRef]
23. Khalaghi, B.; Kvalheim, E.; Tokushige, M.; Teng, L.; Seetharaman, S.; Haarberg, G.M. Electrochemical behavior of dissolved iron chloride in KCl + LiCl + NaCl melt at 550 °C. *ECS Trans.* **2014**, *64*, 301–310. [CrossRef]
24. Tang, H.; Pesic, B. Electrochemical behavior of LaCl3 and morphology of La deposit on molybdenum substrate in molten LiCl–KCl eutectic salt. *Electrochim. Acta* **2014**, *119*, 120–130. [CrossRef]
25. Gibilaro, M.; Massot, L.; Chamelot, P. Investigations of Zr(IV) in LiF-CaF_2, stability with oxide ions and electroreduction pathway on inert and reactive electrodes. *Electrochim. Acta* **2013**, *95*, 185–191. [CrossRef]
26. Hu, H.; Gao, Y.; Lao, Y. Yttria-Stabilized Zirconia Aided Electrochemical Investigation on Ferric Ions in Mixed Molten Calcium and Sodium Chlorides. *Metall. Mater. Trans. B* **2018**, *49*, 2749–2808. [CrossRef]
27. Li, H.; Jia, L.; Liang, J.L.; Yan, H.Y.; Cai, Z.Y.; Reddy, R.G. Study on the Direct Electrochemical Reduction of Fe_2O_3 in NaCl-$CaCl_2$ Melt. *Int. J. Electrochem. Sci.* **2019**, *14*, 11267–11278. [CrossRef]
28. Li, Y.; Li, N.; Miao, W.K.; Wang, C.X.; Kuang, D.Z.; Han, S.M. Nd–Mg–Ni alloy electrodes modified by reduced graphene oxide with improved electrochemical kinetics. *Int. J. Miner. Metall. Mater.* **2020**, *185*, 119–128. [CrossRef]
29. Yan, X.Y.; Fray, D.J. Production of niobium powder by direct electrochemical reduction of solid Nb_2O_5 in a eutectic $CaCl_2$-NaCl melt. *Metall. Mater. Trans. B* **2002**, *33*, 685–693. [CrossRef]
30. Sri, M.; Sanil, N.; Shakila, L.; Panneerselvam, G.; Sudha, R.; Mohandas, K.S.; Nagarajan, K. A study of the reaction pathways during electrochemical reduction of dense Nb_2O_5 pellets in molten $CaCl_2$ medium. *Electrochim. Acta* **2013**, *100*, 51–62.
31. Xiao, W.; Jin, X.; Deng, Y.; Wang, D.; Hu, X.; Chen, G.Z. Electrochemically driven three-phase interlines into insulator compounds, electroreduction of solid SiO_2 in molten $CaCl_2$. *Chemphyschem* **2010**, *7*, 1750–1758. [CrossRef] [PubMed]
32. Kjos, O.S.; Haarberg, R.M.; Martinez, A.M. Electrochemical Production of Titanium from Oxycarbide Anodes. *Key Eng. Mater.* **2010**, *436*, 93–101. [CrossRef]
33. Mohandas, K.S.; Fray, D.J. Electrochemical Deoxidation of Solid Zirconium Dioxide in Molten Calcium Chloride. *Metall. Mater. Trans. B* **2009**, *40*, 685–699. [CrossRef]
34. Zhong, M.; Yang, X.; Yasuda, K.; Homma, T.; Nohira, T. Effect of Si Addition on the Electrochemical Reduction Rate of SiO_2 Granules in Molten $CaCl_2$. *Metall. Mater. Trans. B* **2018**, *49*, 341–348. [CrossRef]
35. Caban, K.; Donten, M.; Stojek, Z. Electroformation of Microlayers of Ionic Liquids in Undiluted Nitromethane and Its Homologues. Unusual Oscillations behind the Range of Limiting Steady-State Current. *J. Phys. Chem. B* **2004**, *108*, 1153–1159.
36. Chen, S.M.; Liao, C.F.; Lin, J.Y.; Cai, B.Q.; Wang, X.; Jiao, Y.F. Electrical conductivity of molten LiF–DyF_3–Dy_2O_3–Cu_2O system for Dy–Cu intermediate alloy production. *Int. J. Miner., Metall. Mater.* **2019**, *26*, 701–709. [CrossRef]